Three-dimensional dual-polarized frequency selective structure with wide out-of-band rejection

Li, Bo; Shen, Zhongxiang

2013

Li, B., & Shen, Z. (2014). Three-Dimensional Dual-Polarized Frequency Selective Structure With Wide Out-of-Band Rejection. IEEE Transactions on Antennas and Propagation, 62(1), 130-137.

https://hdl.handle.net/10356/103920

https://doi.org/10.1109/TAP.2013.2287000

Three-Dimensional Dual-Polarized Frequency Selective Structure with Wide Out-of-Band Rejection

Bo Li and Zhongxiang Shen, *Senior Member, IEEE*

***Abstract*—A new three-dimensional bandpass frequency-selective structure (FSS) is proposed for dual-polarized applications. Each square unit cell of the proposed FSS consists of vertical and horizontal double-sided parallel-strip lines (DSPSLs) and a thin metallic plate. Furthermore, the parallel-strip lines of every DSPSL are connected together through via holes. Using this arrangement, multimode resonators are established in the proposed structure. At lower frequencies, the substrate mode propagates and two resonators along the DSPSL are constructed, leading to a bandpass response with two transmission poles. At higher frequencies, the air mode is reflected by and resonates along the inserted plate, resulting in a stopband with two transmission zeros. The operating principle for this FSS is explained with the aid of an equivalent circuit model. Moreover, a parametric study of the proposed FSS is also carried out and design guidelines are formulated. As an example, a prototype of the proposed FSS is designed, fabricated, and tested. Measured results demonstrate that the FSS exhibits dual polarizations, high out-of-band rejection, and stable frequency response under both transverse electric (TE) and transverse magnetic (TM) polarizations of an obliquely incident wave.**

***Index Terms*—Double-sided parallel-strip line, dual-polarization, frequency-selective structure.**

I. Introduction

Traditional frequency-selective surfaces, which are normally made of a two-dimensional (2-D) periodic arrangement of identical unit cells (such as patches, strips, apertures, slots, and the like), have been widely investigated [1], [2]. Unfortunately, most of these single-layer 2-D frequency-selective surfaces suffer from poor filtering characteristics, such as poor selectivity and unstable angular response. Subsequently, several novel multilayer and three-dimensional (3-D) frequency-selective surfaces were proposed to alleviate the above-mentioned shortcomings of traditional 2-D surfaces [3]-[7]. A bandpass frequency-selective surface by integrating two patch antenna arrays and one array of non-radiating resonant structures in between was described in [3]. Multiple transmission poles in the passband were obtained and one transmission zero was produced in the lower rejection band. The flatness of the passband was thus improved and a fast roll off in the rejection band was obtained. Another type of frequency-selective surface with high selectivity was presented by using multilayer topology in [4], [5]. An additional transmission zero near the passband was created by introducing an extra series *LC* resonator in one of the layers. In [6] and [7], several frequency-selective surfaces based on substrate integrated waveguides (SIWs) were proposed and quasi-elliptic filtering responses were achieved by introducing cross couplings between SIW cavities and slots etched on the top and bottom surfaces of these SIWs. A 3-D frequency selective surface made of an array of circular tubes was described in [8], where the frequency response was mainly determined by the tube thickness.

Recently, a novel concept of 3-D frequency-selective structure (FSS) was reported in [9], where multiple transmission zeros/poles can be produced by a 3-D FSS with multimode cavities/resonators. Compared to 2-D surfaces, the filtering responses of 3-D FSSs can be greatly improved by introducing transmission zeros/poles at desired frequencies. Based on this concept, a new type of 3-D FSS consisting of a 2-D periodic array of vertical microstrip line resonators was proposed in [10]-[12] to achieve quasi-elliptic bandstop filtering response. Transmission poles and zeros were realized by using resonances and couplings of two quasi-transverse electromagnetic (TEM) modes excited by the shielded microstrip line. On the other hand, by combing this microstrip-line array with an array of rectangular waveguide resonators, a quasi-elliptic bandpass FSS with two transmission poles and two transmission zeros located near the passband was realized in [13]. Although quasi-elliptic bandpass responses were observed in [3]-[7], [13], these designs cannot achieve wideband out-of-band rejection together with high selectivity, which is actually desired in many practical applications. Furthermore, the FSSs presented in [9]-[13] only operate under a single polarization, which further limits their applications.

In this paper, a new 3-D bandpass FSS with wide stopband characteristic is presented for dual-polarized applications. In each unit cell, multimode resonators for both transverse electric (TE) and transverse magnetic (TM) polarizations are constructed by using two printed double-sided parallel-strip lines (DSPSLs): one pair in the horizontal direction and another pair in the vertical direction, as well as an inserted metallic plate. At lower frequencies, signals can pass through the structure and a bandpass response with a transmission pole is realized around the resonant frequency of the DSPSL. Besides, the parallel strip lines of each DSPSL are connected together, which can introduce one more resonator in the passband leading to a wider bandwidth. The inserted metallic plate in the air region is employed to provide another two resonators that produce two transmission zeros at higher frequencies. A practical realization of the proposed FSS operating at the center frequency of 7.5 GHz is designed. Under the normal incidence,

Manuscript received December 12, 2012.

The authors are with the School of Electrical and Electronic Engineering, Nanyang Technological University, 50 Nanyang Avenue, Singapore 639798 (e-mail: ezxshen@ntu.edu.sg).

the designed FSS has a relative 3-dB passband bandwidth of 18.4% and a bandwidth of about 78.4% for the out-of-band rejection better than 20 dB.

II. Description of The FSS and DSPSL

A. Description of the FSS

The proposed 3-D FSS, illustrated in Fig. 1(a), consists of two arrays of vertically and horizontally placed DSPSLs and a number of inserted metallic plates. Figs. 1(b) and (c) show the structural details of a square unit cell, where the dash line represents the periodic boundary. It is seen that the two parallel strip lines of each DSPSL are connected together by a centered via hole. In addition, a square and thin metallic plate is inserted in the air region, which is in contact with the inner strip lines. Periods along the *x*- and *y*-axes are denoted by *b*. The thicknesses of the proposed FSS and the inserted metallic plate along the *z*-axis are represented by *l* and l_m, respectively. The distances between the metallic plate and two ends of the DSPSL are l_3 and l_4. The line width of each strip line and the diameter of the via hole are *w* and *D*, respectively. It is noted that the horizontal and vertical DSPSLs have the same topology and dimension, and they are responsible for TE and TM polarizations of the incident wave, respectively. It is therefore seen that the proposed FSS is insensitive to the polarization of an incoming wave under the normal incidence. In the following sections, we will only discuss the operating principle for the horizontally placed DSPSL under the normal incidence.

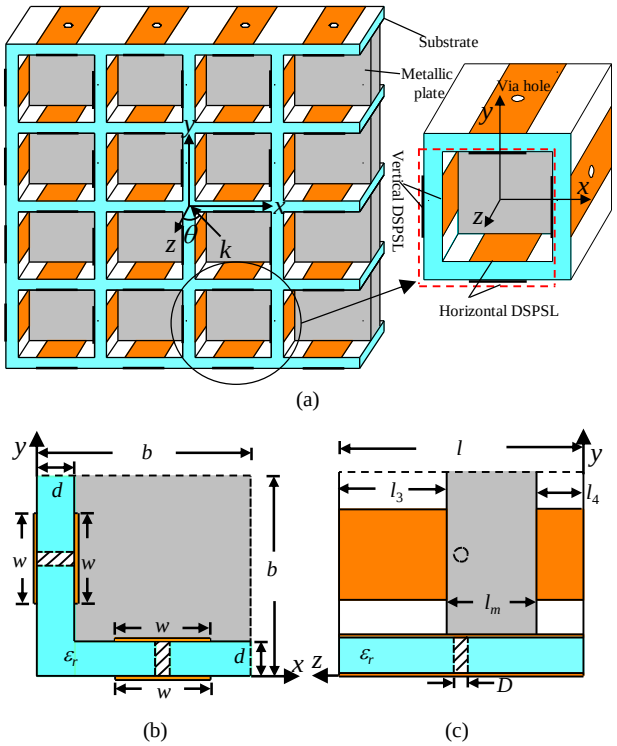

Fig. 1. Geometry of the proposed FSS consisting of vertically and horizontally placed DSPSLs and inserted metallic plates. (a) Perspective view of the proposed FSS and one unit cell; (b) Front view of a unit cell in the *xy* plane; (c) Side view of a unit cell in the *yz* plane.

B. Double-Sided Parallel-Strip Line

Fig. 2 shows the cross-section and electric (E-) field distribution of a DSPSL, which comprises two identical strip lines, one on the top layer of the substrate and the other on the bottom. According to the descriptions in [14] and [15], a DSPSL can be considered as a printed finite conductor parallel plate waveguide, which supports quasi-TEM waves. Furthermore, the quasi-TEM field distribution remains unchanged if a virtual ground plane with infinite extent is inserted at the center of the substrate and parallel to the strip conductors, as shown in Fig. 2. Therefore, the DSPSL can be considered as a combination of two identical back-to-back microstrip lines and the DSPSL has similar characteristic to that of microstrip lines [15]. Compared with a microstrip line, a DSPSL has several advantages: (i) it has wider line width than a microstrip line with the same characteristic impedance; (ii) it gives shorter wavelength than a microstrip line with the same line width. In this design, the DSPSL is employed not only based on the above two advantages, but also its propagating quasi-TEM modes in the entire frequency range. If DSPSLs are replaced with traditional microstrip lines, the ground plane of horizontal and vertical microstrip lines will connect together and they may form a dielectric-filled square waveguide, which is more dispersive. The proposed FSS is somehow similar to the structure described in [13]. However, waveguide modes are excited and propagate in the structure described in [13], thus resulting in narrow bandwidth and also narrow out-of-band rejection.

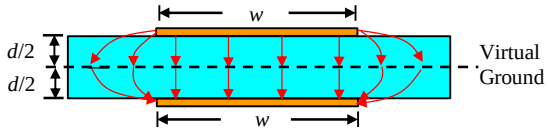

Fig. 2. E-field lines on the cross section of a DSPSL.

III. The Operating Principle

It may be useful to recall the structure presented in [10] and its operating principle. When the E-field of an incident plane wave is perpendicular to the strip lines, two propagating paths, the air and substrate paths, are formed along the shielded microstrip lines. Correspondingly, air and substrate quasi-TEM modes are excited and propagate in the two paths, respectively. At lower frequencies, most signals go from one port to the other through the air path, thus leading to a lowpass response. At higher frequencies, signals can pass through both paths. Owing to the fact that the guided wavelength of substrate mode is smaller than that of air mode, signals coupled through two paths will have a phase difference. Transmission zeros are then obtained at frequencies where the two propagating modes are combined out of phase. Transmission poles are produced when the individual length of the air or substrate mode reaches approximately half a guided wavelength.

In each unit cell of the present design, two horizontal and vertical via holes are introduced at the center of the corresponding DSPSLs and a metallic plate is inserted in the air region, which are different from the structure in [10]. The substrate propagating path still exists through DSPSLs, which

means that the substrate quasi-TEM mode can also be excited and propagate though it may be perturbed by the introduced via holes. However, the air propagating path is blocked by the inserted metallic plate because signals coupled to the air path will be reflected by the inserted metallic plate. Therefore, the air quasi-TEM mode may not link the input and output ports though they may still be excited. Transmission zeros are then achieved at frequencies where the air mode meets their resonant conditions. Compared with the structure in [10], the present FSS can provide more resonators in the operating frequency range and has very different filtering response. Fig. 3 shows the simulated S-parameter results of the proposed FSS, where a good bandpass filtering response with a wide stopband at higher frequencies can be observed under the normal incidence.

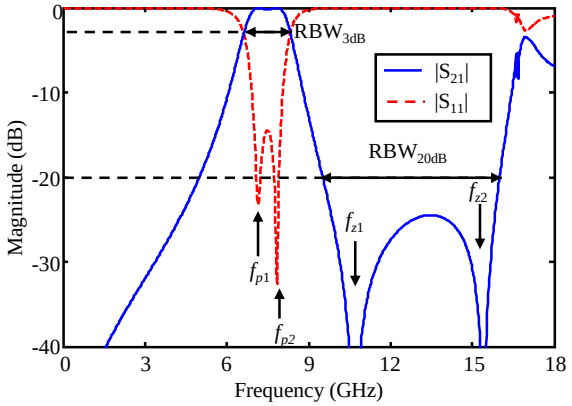

Fig. 3. Simulated S-parameter results of the proposed bandpass FSS using full-wave EM simulator CST-MWS (b = 8.0 mm, w = 4.0 mm, l = 12 mm, l_3 = 4.65 mm, l_4 = 3.05 mm, D = 1.7 mm, ε_r = 3.0, d = 1.524 mm, TE incidence, θ = 0°).

A. Resonant Characteristics of the Substrate Mode

As discussed above, only the substrate propagating path along DSPSL exists linking the input and output ports of the proposed FSS. At a very low frequency, although most signals are coupled to the substrate path due to the existence of the metallic plate, the proposed FSS still exhibit strong reflection because the two parallel strip lines are connected by a via hole. However, the DSPSL section will resonate when the frequency increases to a certain value. A passband with two transmission poles can then be obtained around the resonant frequencies of the DSPSL with the via hole, as shown in Fig. 3. The propagating and resonant characteristics of the FSS can be explained by an equivalent circuit model shown in Fig. 4. It is seen that the equivalent circuit model contains two series sub-networks representing the air and substrate paths. In the substrate path, the DSPSL is represented by a transmission line with equivalent characteristic impedance Z_d and electrical length θ_l. The coupling between the input/output ports and the DSPSL is denoted by capacitor C_d. The inductor L denotes the effect of the via hole connecting the two strip lines of a DSPSL.

The E-field lines of a DSPSL (in the *yz* plane) at the two resonant frequencies f_{p1} and f_{p2} are shown in Figs. 5(a) and (b). It is seen that, at resonant frequency f_{p1}, the E-field vectors of the DSPSL have the same magnitude and direction at both sides of the via hole, which means the transmission pole at f_{p1} is produced by the resonance between half of the DSPSL and the via hole. In the equivalent circuit model, this resonator can be represented by R_1, which can also be seen as a short-circuited transmission line resonator [16]. At resonant frequency f_{p2}, the E-field vectors at both sides of the via hole along the DSPSL still have the same magnitude but opposite directions, which means the transmission pole at f_{p2} is provided by the resonance of the entire DSPSL. In the equivalent circuit model, this resonance is denoted by resonator R_2, which can be equivalent to an open-circuited transmission line resonator [16].

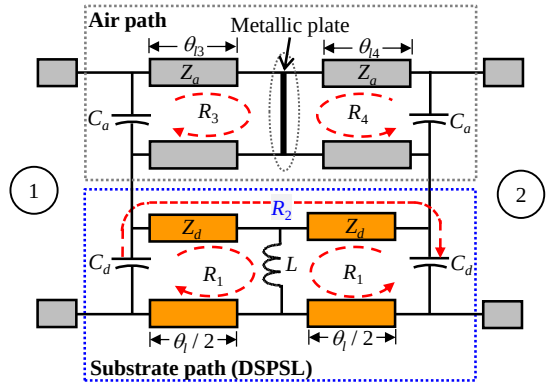

Fig. 4. Equivalent circuit model of the proposed FSS.

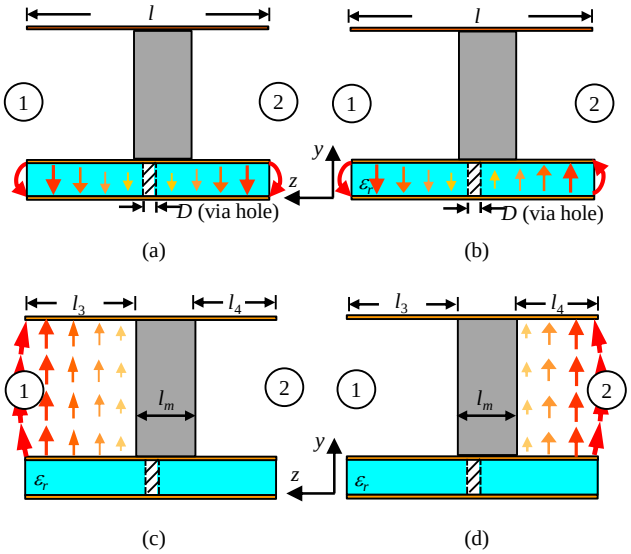

Fig. 5. (a) and (b) E-field distributions for the substrate mode at frequencies f_{p1} and f_{p2}; (c) and (d) E-field distributions for the substrate mode at frequencies f_{z1} and f_{z2}.

B. Resonant Characteristics of the Air Mode

It is understood that the inserted metallic plate is used to reflect signals coupled to the air path. As shown in Fig. 1(c), the metallic plate divides the air region into two parts (the left and right sides of the air region), both of which can resonate at frequencies above the passband because the wavelength in the air region is relatively longer than that in the substrate. When the left (right) side resonates, all the signals coupled to this region are reflected, thus leading to a transmission zero at f_{z1} (f_{z2}). Figs. 5(c) and (d) sketch the E-field vectors of the resonant

modes at frequencies f_{z1} and f_{z2}. It is seen that the *E*-field vectors coupled from the input ports and then decreases to zero when these signals reach the metallic wall. The resonant characteristics of this case can also be explained by the equivalent circuit model shown in Fig. 4. In the air path of this equivalent circuit, two transmission-line sections (Z_a, θ_{l3}) and (Z_a, θ_{l4}) denote the left and right sides of the separated air path, respectively. Z_a is the equivalent characteristic impedance of the air mode; θ_{l3} and θ_{l4} are the electrical lengths of the left and right sides of the air path. Due to the coupling between vertical and horizontal DSPSLs, the equivalent characteristic impedance Z_a is lower than the standalone impedance. The inserted metallic plate is represented by a short circuit between (Z_a, θ_{l3}) and (Z_a, θ_{l4}). The discontinuity between the input/output ports and the air region of the presented FSS is denoted by capacitor C_a. As discussed earlier, both transmission-line sections (Z_a, θ_{l3}) and (Z_a, θ_{l4}) will resonate and produce transmission zeros at frequencies above the passband. In order to facilitate the description, resonators R_3 and R_4 shown in Fig. 4 are used to represent the resonant characteristics of transmission-line sections (Z_a, θ_{l3}) and (Z_a, θ_{l4}). It should be clear that R_3 and R_4 can be seen as two short-circuited transmission line resonators. More detailed simulation results can be found in the parametric analysis in Section IV.

IV. Parametric Study and Design Guidelines

A. Parametric Study

In order to establish a generally applicable design procedure for the proposed FSS, a parametric study is conducted. The analysis is carried out by simulating different variations of the proposed structure with the help of the full-wave simulator CST MWS. As shown in Fig. 3, there are six specifications when designing this FSS: two transmission-pole frequencies f_{p1} and f_{p2}, two transmission-zero frequencies f_{z1} and f_{z2}, RBW_{3dB} and RBW_{20dB}. RBW_{3dB} and RBW_{20dB} are defined as follows:

$$RBW_{3dB} = \frac{\text{Bandwidth of } |S_{21}| \geq \text{-3dB}}{[(f_{p1} + f_{p2})/2]} \times 100\% \quad (1)$$

$$RBW_{20dB} = \frac{\text{Bandwidth of } |S_{21}| \leq \text{-20dB}}{[(f_{p1} + f_{p2})/2]} \times 100\% \quad (2)$$

where RBW_{3dB} represents relative 3-dB bandwidth of the passband and RBW_{20dB} denotes 20-dB relative bandwidth of out-of-band rejection in higher frequencies.

Figs. 6(a) and (b) show the variation of resonant frequencies and bandwidths with respect to the diameter *D* of the via hole and the width *w* of DSPSL, respectively. It is seen from Fig. 6(a) that *D* only affects the resonant frequency f_{p1} and a smaller *D* leads to a lower f_{p1}. This can be explained by the equivalent circuit model in Fig. 4. The inductance *L* is mainly determined by *D*, which is only included in resonator R_1. Therefore, the resonant frequency f_{p1} varies with *D*, while other resonant frequencies remain more or less the same. Furthermore, the bandwidth of passband (RBW_{3dB}) increases first and then decreases with a growing *D*. When *D* is small, f_{p1} is much lower than f_{p2} and the structure exhibits a dual-band bandpass response, thus leading to a narrow bandwidth. When *D* is very large, f_{p1} and f_{p2} may merge together, which obviously results in a narrow bandwidth. As observed in Fig. 6(b), all of the resonant frequencies will change when *w* varies. This is because the strip line is present in all of the resonators R_1, R_2, R_3 and R_4. The frequencies f_{p1} and f_{p2} of transmission poles decrease with an increasing *w*, while the frequencies f_{z1} and f_{z2} of transmission zeros increase. This is because increasing *w* will greatly enlarge the coupling capacitor C_d in resonators R_1 and R_2, thus resulting in lower resonant frequencies. It is also noted that increasing *w* leads to smaller impedance for the strip line, which means the values of Z_d and Z_a, become smaller and so do the electrical lengths of θ_l, θ_{l3} and θ_{l4}. Therefore, the resonant frequencies f_{z1} and f_{z2} become higher accordingly. Furthermore, both RBW_{3dB} and RBW_{20dB} increase when enlarging *w*, which suggests that *w* should be as larger as possible to obtain wide bandwidths.

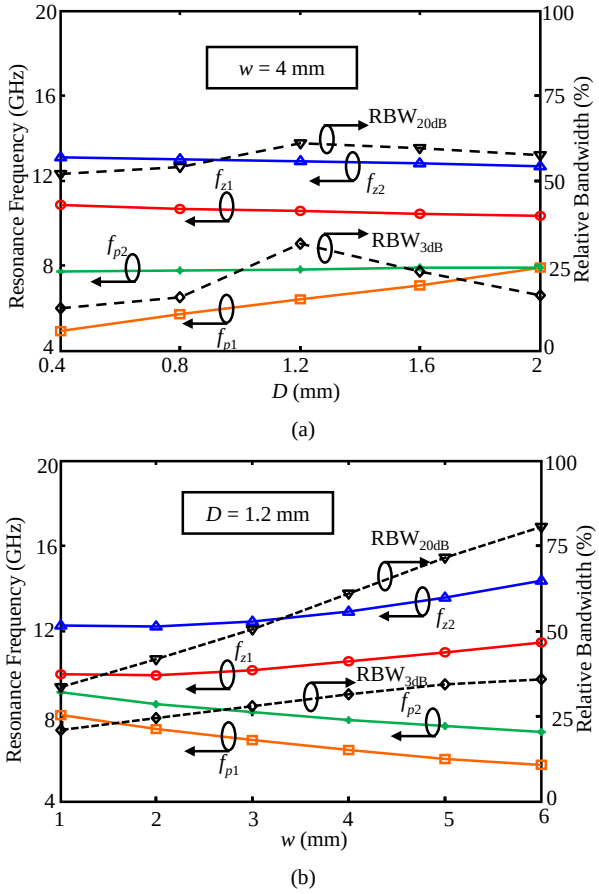

Fig. 6. Variation of resonant frequencies and bandwidths with respect to *D* and *w* (b = 8 mm, l = 12 mm, l_3 = 4.75 mm, l_4 = 3.75 mm, ε_r = 3.0, d = 1.524 mm, TE incidence, θ = 0°).

Fig. 7 shows the resonant frequencies and relevant bandwidths under different values of l_3 or l_4 ($l_{3(4)}$). It is seen that when adjusting $l_{3(4)}$, the frequencies f_{p1} and f_{p2} remain almost unchanged, while those of transmission zeros vary accordingly. This is because l_3 and l_4 are only related to resonators R_3 and R_4 respectively, which have no influence on R_1 and R_2. As seen in Fig. 7, when increasing l_3 while fixing l_4 = 4.5 mm, f_{z1} is lowered significantly, while f_{z2} is unchanged at around 11.85

GHz. The same situation can be observed for f_{z2} when adjusting l_4 and fixing l_3 = 4.5 mm. This means that the two transmission zeros provided by resonators R_3 and R_4 can be adjusted independently while retaining the passband performance, which provides more freedom for the FSS design. It should be noted that when $l_3 = l_4$ = 4.75 mm, the metallic plate is placed at the middle of the DSPSL and the two transmission zeros are merged into one, as shown in Fig. 7. This is understandable because R_3 and R_4 have the same length, resulting in the same resonant frequency. Furthermore, it should be mentioned that f_{z1} and f_{z2} may not be adjusted too far away from each other for a large $\mathrm{RBW}_{20\mathrm{dB}}$ because the ripple in the stopband will become noticeable. Therefore, l_3 and l_4 should be properly adjusted to achieve a wider bandwidth for the out-of-band rejection.

Fig. 8 shows resonant frequencies and bandwidths as functions of period b and thickness l of the proposed FSS. It is observed that f_{z1} and f_{z2} decrease with increasing b and l, respectively. This is attributed to the fact that the resonant lengths of R_3 and R_4 increase when enlarging b and l. The frequency f_{p1} decreases with an increasing value of b, while f_{p2} increases. This can be explained by the inverse relationship between the strip line's impedance and the coupling between these closely spaced strip lines. The difference between f_{p1} and f_{p2} can then be widened by using a large b. Meanwhile, $\mathrm{RBW}_{20\mathrm{dB}}$ decreases with a large b, while it increases with an increasing l. Moreover, $\mathrm{RBW}_{3\mathrm{dB}}$ increases initially and then decreases when b increases. This is expected because when b is too small, f_{p1} and f_{p2} are too close to each other; when b is too large, the difference between f_{p1} and f_{p2} becomes too large and the structure exhibits a dual-band bandpass response, which is similar to the situation when D is small.

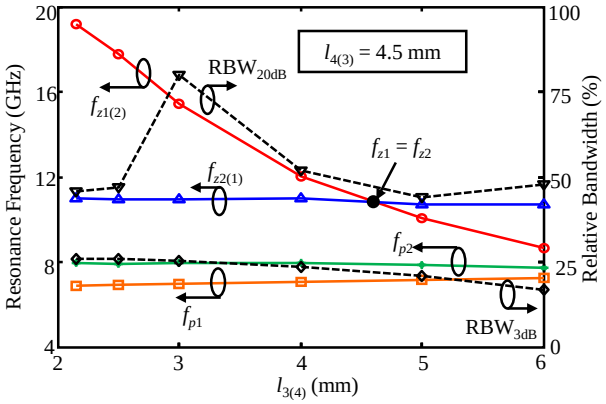

Fig. 7. Variation of resonant frequencies and bandwidths with respect to l_3 or l_4 (b = 8 mm, l = 12 mm, w = 4 mm, D = 1.6 mm, ε_r = 3.0, d = 1.524 mm, TE incidence, $\theta = 0^o$).

B. Design Guidelines

Based on the understanding gained through parametric studies, the following guidelines are suggested for a fast design of the proposed FSS.

- A substrate material with low dielectric constant ε_r may be preferred. Although this may lead to a relative larger and thicker FSS, it is easy to fabricate and assemble the proposed FSS with a less stringent tolerance requirement.
- Period b should be selected much smaller than the operating wavelength for a larger out-of-band rejection bandwidth and stable frequency performance even under a large variation of the angle of incidence. However, b may not be selected too small since it may be difficult and costly to fabricate and assemble the structure.
- The thickness l is approximately equal to $\lambda_g/2$, where λ_g is the wavelength of the quasi-TEM mode at the desired center frequency. λ_g is approximately $c / f_0\sqrt{\varepsilon_{eff}}$, where c is the speed of light in free space, f_0 denotes the desired center frequency, and ε_{eff} represents the effective dielectric constant of the structure.
- Since a large w can lead to a wide bandwidth, the strip width w is chosen to be close to (b - d). Since the diameter D only influences the first transmission pole, it can thus be used as a parameter for obtaining the desired bandwidth for the passband.
- The location and thickness of the metallic plate is determined by l_3 and l_4, which only influence the out-of-band rejection performance in higher frequencies. Decreasing l_3 or l_4 leads to a higher f_{z1} or f_{z2}, and vice versa. l_3 and l_4 can be adjusted individually to obtain a wider bandwidth for out-of-band rejection.

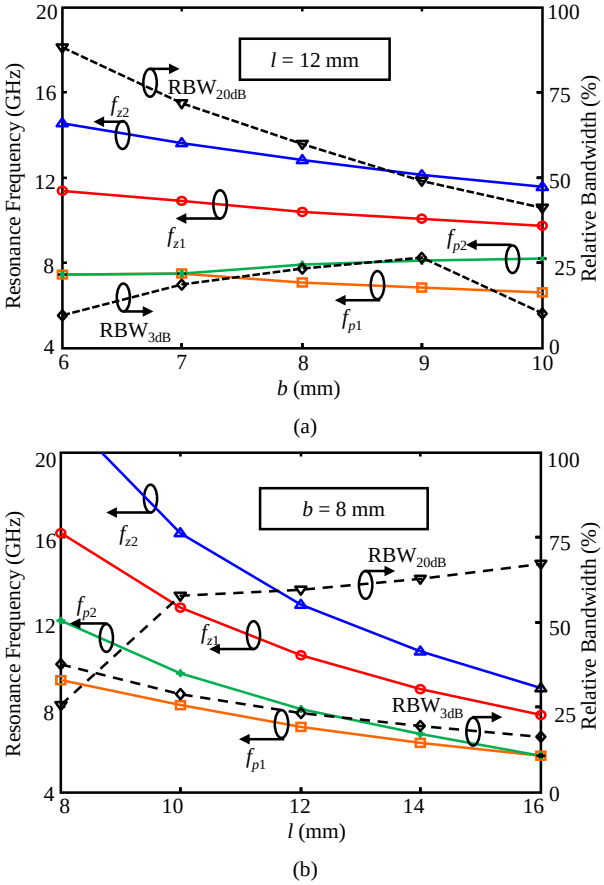

Fig. 8. Variation of resonant frequencies and bandwidths with respect to b and l (l_m = 3.5 mm, w = 4 mm, D = 1.6 mm, ε_r = 3.0, d = 1.524 mm, TE incidence, $\theta = 0^o$).

C. Design Example

A prototype of the proposed bandpass FSS with a center frequency of 7.5 GHz is designed. The transmission-pole and transmission-zero frequencies are designed to be f_{p1} = 7.1, f_{p2} = 7.9, f_{z1} = 10.5, and f_{z2} = 15.3 GHz, respectively. In this design, all the DSPSLs are printed on a substrate of Rogers 4230 (ε_r = 3.0, d = 1.524 mm, tanδ = 0.0023). The thickness of the copper on both sides of the substrate is 1*oz*. The dimensions of the FSS unit cell are as follows: b = 8.0 mm, w = 4.0 mm, l = 12 mm, l_3 = 4.65 mm, l_4 = 3.05 mm, D = 1.7 mm.

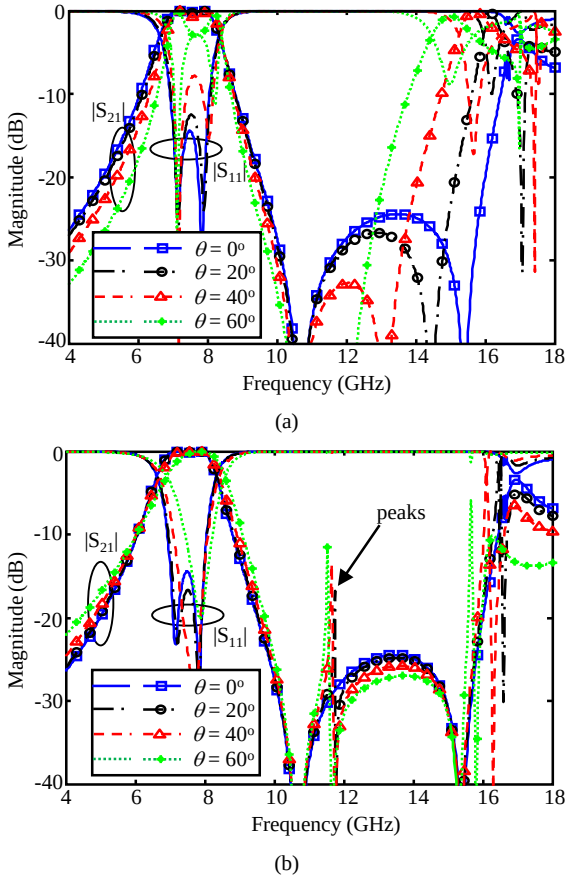

Fig. 9. Simulated results of the designed FSS under oblique incidence angles for (a) TE polarization and (b) TM polarization.

Fig. 9 illustrates the simulated S-parameter results of the designed FSS for both TE and TM polarizations under various incident angles. It is observed that under TE polarization, the ripple in the passband increases with the growing incident angle, which is mainly attributed to the decrease of the wave impedance of the incidence wave seen at the striking interface for a large incident angle [1]. RBW_{3dB} decreases from 22.9% to 19.7% when the incident angle increases from 0° to 60°. Meanwhile, the transmission zero at f_{z1} is very stable when the incident angle varies. However, the frequency f_{z2} reduces with the increasing incident angle, thus leading to a reduced bandwidth for the out-of-band rejection. When the incident angle increases from 0 to 60°, RBW_{20dB} varies from 86.3% to 51.1%. Under TM polarization, the passband ripple decreases slightly as the incident angle increases. This is mainly because the wave impedance of the incidence wave increases a little in this case [1]. RBW_{3dB} varies from 22.9% to 21.4% when the incident angle increases from 0° to 60°. Although the transmission zeros and the bandwidth of the stopband are stable, a parasitic peak (around 12 GHz) in the stopband occurs under oblique incidence, as shown in Fig. 9(b). This peak can be attributed to the coupling of two closely placed vertical and horizontal strips because the E-field vectors have longitudinal components under TM polarization and oblique incidence.

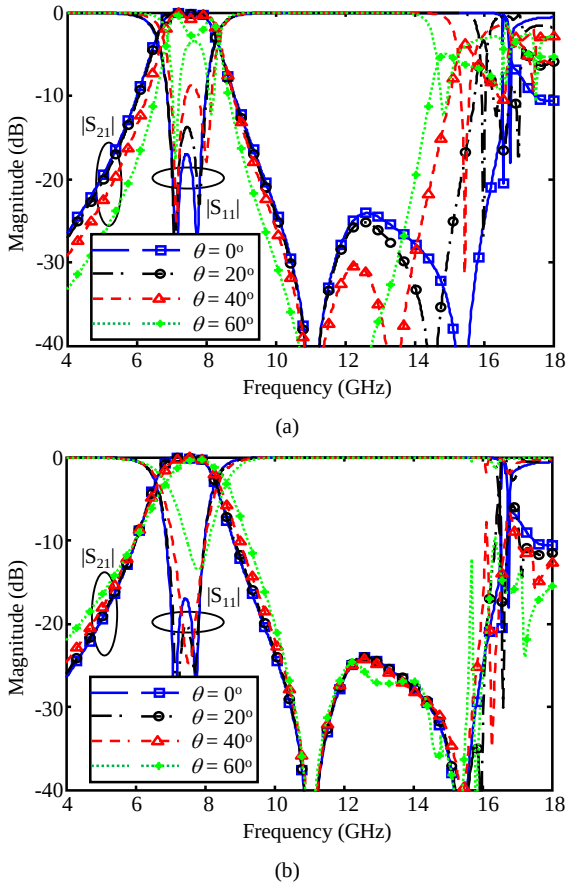

Fig. 10. Simulated results of the proposed FSS with loading stubs under oblique incidence angles for (a) TE polarization and (b) TM polarization.

In this design, two small stubs with the same dimensions are introduced to connect the vertical and horizontal strips to remove these peaks under TM polarization and oblique incidence. Fig. 10 shows the simulated S-parameter results of the modified FSS with two loading stubs. It is seen that the filtering responses under TE polarization remain unchanged with and without loading stubs. Under TM polarization and oblique incidence, the filtering responses change slightly except that these peaks in the stopband disappear. The location and line width of this stub can be optimized and its effect may be carefully accounted for. In this design, the length and width of each stub are optimized to be 1.2 mm and 0.2 mm respectively, as shown in Fig. 11.

V. Implementation and Measured Results

A. Implementation

Fig. 11 shows the implementation and assembly details of a

unit cell in our design. The DSPSLs are printed on the Rogers 4230 substrate and are cut into 2-D pieces, as shown in Fig. 12(b). These horizontal and vertical 2-D pieces are cross-joined together to form the required structure through the slots cut half way along the circuit board. Furthermore, in every unit cell, the subs for cancelling coupling between DSPSLs under TM polarization are in good contact after vertical and horizontal circuit boards cross-inserted. Additionally, the metallic plate for providing transmission zeros is realized using aluminum due to its light weight. As discussed above, the location of the aluminum plate is a very important parameter for resonant frequencies in the stopband and this plate should be fixed tightly. In this realization, this aluminum plate is secured in the unit cell by using four short metallic rods, which go through the via holes in the circuit board and extend into the aluminum plate, as shown in Fig. 11.

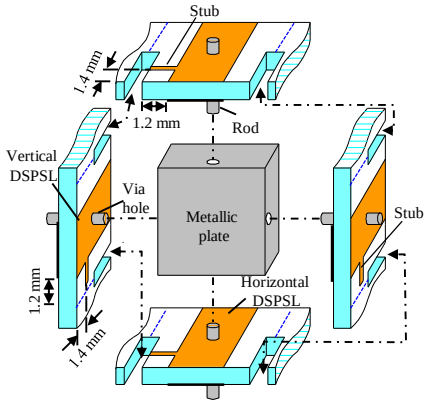

Fig. 11. Assembly details of pieces forming one unit cell.

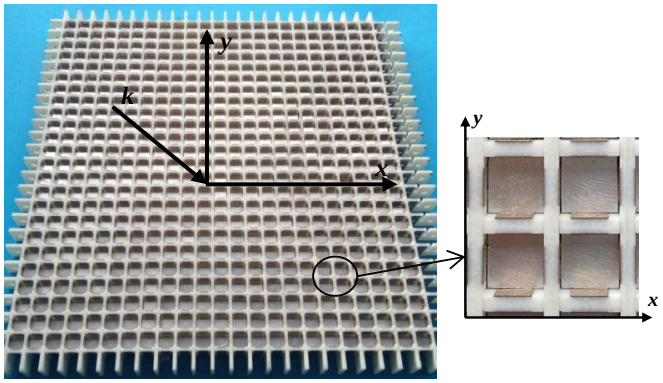

(a)

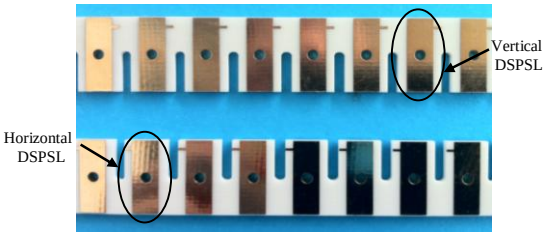

(b)

Fig. 12. Photographs of the fabricated FSS. (a)Perspective view; (b) Top view of the fabricated DSPSLs.

B. *Measured Results*

Fig. 12 shows the photo of our fabricated prototype, which is approximately 185 mm × 193 mm in size and consists of 552 unit cells. Both transmission and reflection coefficients are measured by the free-space method using two horn antennas in an anechoic chamber, similar to the measurement set-up described in [13]. Fig. 13 shows measured and simulated S-parameter results of the fabricated FSS under different (TE and TM) polarizations and incident angles (0^o, 20^o and 40^o). It is observed that the frequency performance of the proposed FSS is very stable under different incident angles. Furthermore, it is seen that the fabricated FSS can successfully provide a passband with two transmission poles at 7.4 and 7.8 GHz and a stopband with two transmission zeros close to 10 and 14.6 GHz under normal incidence.

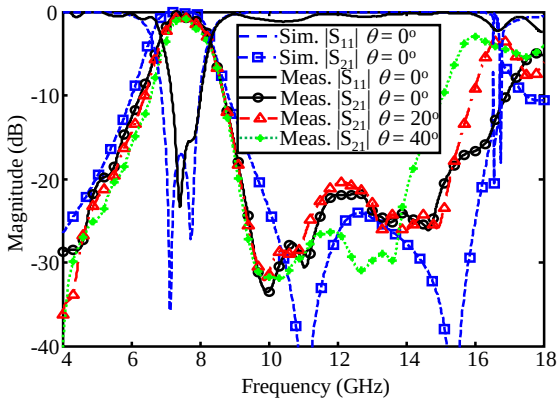

(a)

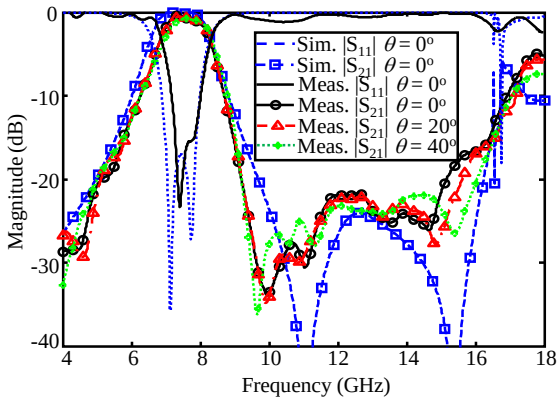

(b)

Fig. 13. Measured results of the fabricated FSS under oblique incidence for (a) TE polarization and (b) TM polarization.

It is observed that measured transmission zero and pole frequencies have small shifts compared to their simulated ones. Such discrepancies between measured and simulated results are attributed to assembly errors. Due to these errors, the measured RBW_{3dB} is 18.4%, which is slightly narrower than the simulated one (22.9%). The measured RBW_{20dB} is 78.4% under normal incidence. In addition, the measured insertion loss at the center frequency of the passband is 0.72 dB under the normal incidence, which is greater than the simulated one (0.13 dB). A larger measured insertion loss may be due to the surface

roughness of the fabricated aluminum plates and the connection loss between aluminum plates and strips printed on substrates. Moreover, when the incident angle increases up to 40^{o}, the measured insertion loss at the center frequency increases to 1.1 dB for TE polarization, and it varies to 0.9 dB for TM polarization.

VI. Conclusion

This paper has presented a new 3-D dual-polarized frequency-selective structure with wide stopband response. The good bandpass response has been realized through substrate modes, which propagate through a 2-D periodic array of double-sided parallel-strip lines. The wideband rejection has been provided by the resonances of air modes due to the inserted metallic plate. The operating principle of the proposed FSS has been explained through equivalent circuit models and the designed FSS has been successfully verified by measured results.

References

[1] T. K. Wu, *Frequency Selective Surfaces and Grid Arrays*. New York: Wiley, 1995.

[2] B. A. Munk, *Frequency Selective Surfaces: Theory and Design*. New York: Wiley, 2000.

[3] A. Abbaspour-Tamijani, K. Sarabandi, and G. M. Rebeiz, "Antenna-filter-antenna arrays as a class of bandpass frequency-selective surfaces," *IEEE Trans. Microwave Theory Tech.*, vol. 52, no. 8, pp. 1781-1789, Aug. 2004.

[4] M. A. Al-Joumayly and N. Behdad, "Low-profile, highly-selective, dual-band frequency selective surfaces with closely spaced bands of operation," *IEEE Trans. Antennas Propag.*, vol. 58, no. 12, pp. 4042-4050, Dec. 2010.

[5] M. Li and N. Behdad, "A third-order bandpass frequency selective surface with a tunable transmission null," *IEEE Trans. Antennas Propag.*, vol. 60, no. 4, pp. 2109-2113, Apr. 2012.

[6] G. Q. Luo, W. Hong, Z.-C. Hao, B. Liu, W. D. Li, J. X. Chen, H. X. Zhou, and K. Wu, "Theory and experiment of novel frequency selective surface based on substrate integrated waveguide technology," *IEEE Trans. Antennas Propag.*, vol. 53, no. 12, pp. 4035-4043, Dec. 2005.

[7] G. Q. Luo, W. Hong, Q. H. Lai, K. Wu, and L. L. Sun, "Design and experimental verification of compact frequency-selective surface with quasi-elliptic bandpass response," *IEEE Trans. Microwave Theory Tech.*, vol. 55, no. 12, pp. 2481-2487, Dec. 2007.

[8] S. N. Azemi, K. Ghorbani, and W. S. T. Rowe, "3D frequency selective surfaces," *Progress in Electromagnetics Research C*, vol. 29, pp.191-203, 2012.

[9] A. K. Rashid and Z. Shen, "Three-dimensional frequency selective surfaces," presented at the *Int. Conf. Communications, Circuits, and Systems (ICCCAS)*, China, Jul. 2010, pp. 688-691.

[10] A. K. Rashid and Z. Shen, "A novel band-reject frequency selective surface with pseudo-elliptic response," *IEEE Trans. Antennas Propag.*, vol. 58, no. 4, pp. 1220–1226, Apr. 2010.

[11] A. K. Rashid and Z. Shen, "Scattering by a two-dimensional periodic array of vertically placed microstrip lines," *IEEE Trans. Antennas Propag.*, vol. 59, no. 7, pp. 2599-2606, July 2011.

[12] B. Li and Z. Shen, "Miniaturized bandstop frequency-selective structure using stepped-impedance resonators," *IEEE Antennas Wireless Propag. Lett.*, vol. 11, pp. 1112-1115, 2012.

[13] A. K. Rashid, Z. Shen, and B. Li, "An elliptical bandpass frequency selective structure based on microstrip lines," *IEEE Trans. Antennas Propag.*, vol. 60, no. 10, pp. 4661-4669, Oct. 2012.

[14] S.-G. Kim and K. Chang, "Ultrawide-band transitions and new microwave components using double-sided parallel-strip lines," *IEEE Trans. Microwave Theory Tech.*, vol. 52, no. 9, pp. 2148-2152, Sep. 2004.

[15] L. Chiu, Q. Xue, and C. H. Chan, "Performance enhancement of microwave circuits using parallel-strip line," *IEEE Potentials*, vol. 29, no. 5, pp. 16-21, 2010.

[16] J.-S. Hong and M.J. Lancaster, *Microstrip Filter for RF/Microwave Applications*, New York: Wiley, 2001.

Bo Li was born in Hunan, China, in 1984. He received the B.S. and Ph.D. degrees both in communication engineering from Nanjing University of Science and Technology, China, in 2006 and 2011, respectively.

Currently, he is working as a Research Fellow at Nanyang Technological University, Singapore. His research interests include RF/microwave power dividers and frequency-selective surfaces.

Zhongxiang Shen (M'98-SM'04) received the B. Eng. degree from the University of Electronic Science and Technology of China, Chengdu, China, in 1987, the M. S. degree from Southeast University, Nanjing, China, in 1990, and the PhD degree from the University of Waterloo, Waterloo, Ontario, Canada, in 1997, all in electrical engineering.

From 1990 to 1994, he was with Nanjing University of Aeronautics and Astronautics, China. He was with Com Dev Ltd., Cambridge, Canada, as an Advanced Member of Technical Staff in 1997. He spent six months each in 1998, first with the Gordon McKay Laboratory, Harvard University, Cambridge, MA, and then with the Radiation Laboratory, the University of Michigan, Ann Arbor, MI, as a Postdoctoral Fellow. In 1999, he joined Nanyang Technological University (NTU), Singapore, as an assistant professor. He has been an associate professor in the School of Electrical and Electronic Engineering, NTU, since Jan. 2004.

Dr. Shen is a member of the Antennas and Propagation and Microwave Theory and Techniques Societies of the IEEE. He served as Chair of the IEEE MTT/AP Singapore Chapter. He currently serves as the Chair of AP-S Chapter Activities Committee.

His research interests include design of small and planar antennas for various wireless communication systems, analysis and design of frequency-selective structures, hybrid numerical techniques for modeling RF/microwave components and antennas. He has authored or co-authored more than 110 journal papers and another 100 conference papers.